Pressure-induced superconductivity in layered pnictogen diselenide $NdO_{0.8}F_{0.2}Sb_{1-x}Bi_xSe_2$ (x = 0.3 and 0.7)

Ryo Matsumoto,[1,2] Yosuke Goto,[3,*] Sayaka Yamamoto,[1,2,4] Kenta Sudo,[3] Akira Miura,[5] Chikako Moriyoshi,[6] Yoshihiro Kuroiwa,[6] Shintaro Adachi,[1] Tetsuo Irifune,[7] Hiroyuki Takeya,[1] Hiromi Tanaka,[4] Yoshikazu Mizuguchi,[3] and Yoshihiko Takano[1,2]

[1]*National Institute for Materials Science, 1-2-1 Sengen, Tsukuba, Ibaraki 305-0047, Japan*

[2]*University of Tsukuba, 1-1-1 Tennodai, Tsukuba, Ibaraki 305-8577, Japan*

[3]*Department of Physics, Tokyo Metropolitan University, 1-1 Minami-osawa, Hachioji, Tokyo 192-0397, Japan*

[4]*National Institute of Technology, Yonago College, 4448 Hikona, Yonago, Tottori 683-8502, Japan*

[5] *Faculty of Engineering, Hokkaido University, Kita 13, Nishi 8 Sapporo 060-8628, Japan*

[6] *Department of Physical Science, Hiroshima University, 1-3-1 Kagamiyama, Higashihiroshima, Hiroshima 739-8526, Japan*

[7]*Geodynamics Research Center, Ehime University, Matsuyama, Ehime 790-8577, Japan*

*E-mail: y_goto@tmu.ac.jp

Abstract

Polycrystalline samples of layered pnictogen diselenide $NdO_{0.8}F_{0.2}Sb_{1-x}Bi_xSe_2$ (x = 0 to 0.8) were successfully synthesized by solid-state reactions. Electrical resistivity in the synthesized samples was systematically decreased with an increase in Bi content x. Crystal structure analysis using synchrotron X-ray diffraction suggests that insulator to metal transition upon Bi doping correlates with anomalous change in c-axis length and/or corrugation in conducting layer. The emergence of superconductivity under high pressure is demonstrated using diamond anvil cell (DAC) with boron-doped diamond electrodes, for x = 0.3 and 0.7 as the representative samples. For Sb-rich one (x = 0.3), we observed a superconducting transition with T_c^{onset} = 5.3 K at 50 GPa, which is the first-ever report of the superconductivity in layered $SbCh_2$-based (Ch: chalcogen) compounds. The T_c^{onset} of x = 0.3 increased with increasing pressure and reached 7.9 K at 70.8 GPa, followed by the gradual decrease in T_c up to 90 GPa. For Bi-rich one (x = 0.7), a superconducting transition with T_c^{onset} = 5.9 K was observed at 43.5 GPa, which is the almost comparable to that of x = 0.3. The present work will be helpful to bridge the gap between insulating $SbCh_2$-based and metallic $BiCh_2$-based systems, which show superconductivity at ambient pressure.

1. Introduction

Since the discovery of the $BiCh_2$-based (Ch: S, Se) layered superconductors in 2012, such as $Bi_4O_4S_3$ and $R(O,F)BiS_2$ (R: rare-earth element), this family of compounds has received much attention as a new class of layered superconductors [1-8]. The crystal structure is composed of alternate stacks of electrically conducting $BiCh_2$ layers and insulating (blocking) carrier reservoir layers, as schematically depicted in Fig. 1. Several types of $BiCh_2$-based superconductors have been reported, and the highest-record T_c of 11 K was obtained for $LaO_{0.5}F_{0.5}BiS_2$ using high-pressure technique [3,9]. In the early stages of research on a paring mechanism of $BiCh_2$-based compounds, it was suggested that the conventional superconductivity with a fully gapped *s*-wave state is realized, on the basis of the first-principles calculation [10], Raman scattering [11], muon-spin spectroscopy [12], and thermal conductivity [13] experiments. However, recent first-principles calculations [14], angle-resolved photoemission spectroscopy [15], and Se isotope effect [16] proposed the possibility of unconventional pairing mechanisms in $BiCh_2$-based superconductors. Therefore, systematic characterization is still crucial to clarify the superconductivity mechanisms of these compounds.

Generally speaking, the parent phase of $BiCh_2$-based compounds is an *n*-type semiconductor. These compounds show superconductivity when electron carriers are generated at the conduction bands. Because the conduction bands are mainly composed of hybridization between Bi 6*p* and Ch *p* orbitals [17,18], it is quite reasonable to expect that the understanding of the doping effects of Sb for Bi is essentially important to elucidate the superconducting mechanisms and the underlying physics in this family of compounds. Besides superconductivity, Sb doped $BiCh_2$-based

compounds, namely $SbCh_2$-based compounds, are also attractive from the viewpoint of the thermoelectrics and topological materials [19-21]. However, most of $SbCh_2$-based compounds have been insulators so far, in spite of isovalent Sb doping on the Bi site [22-26]. Although the origin of insulating nature in $SbCh_2$-based compounds has not been fully understood yet, it is probably due to insufficient orbital overlapping between Sb 5*p* and Ch *p* orbitals [27]. Indeed, insulator to metal transition was observed for $Ce(O,F)SbS_2$ under high pressure [25].

We have reported the effects of Bi doping on high-temperature thermoelectric transport properties of $SbSe_2$-based layered compounds $NdO_{0.8}F_{0.2}Sb_{1-x}Bi_xSe_2$ ($x \leq 0.4$) [26]. Room temperature electrical resistivity was decreased down from 300 mΩcm for $x = 0$ to 8 mΩcm for $x = 0.4$. However, the temperature dependence of electrical resistivity was still insulating for $x \leq 0.4$. In the present study, we show that Bi-rich composition up to ca. $x = 0.8$ can be obtained by optimizing synthesis temperature. Electrical resistivity in the synthesized samples was systematically decreased with an increase in Bi content *x*. Weakly localized behavior in low temperature electrical transport was still observed for all of examined samples. Electrical transport of $x = 0.3$ and 0.7 was examined under high pressure exceeding 50 GPa using diamond anvil cell (DAC) with boron-doped diamond electrodes. It was found that both samples show superconductivity at low temperature, which is the first-ever report of superconductivity in $SbCh_2$-based layered compounds. Further, the present study is the first report that tunes in a wide range of Bi/Sb content ($x = 0$–0.8). The results enable us to bridge the gap between insulating $SbCh_2$-based and metallic $BiCh_2$-based systems, which shows superconductivity at ambient pressure.

2. Experimental procedures

2.1 Sample preparation

Polycrystalline samples of $NdO_{0.8}F_{0.2}Sb_{1-x}Bi_xSe_2$ (x = 0, 0.1, 0.2, 0.3, 0.4, 0.5, 0.6, 0.7, 0.8) were prepared by solid-state reactions using dehydrated Nd_2O_3, NdSe, $NdSe_2$, Sb (99.9%), Bi (99.999%), and Se (99.999%) as starting materials. The dehydrated Nd_2O_3 was prepared by heating commercial Nd_2O_3 powder (99.9%) at 600ºC for 10 h in air. To obtain the NdSe and $NdSe_2$ mixtures, Nd (99.9%) and Se in a molar ratio of 2:3 were heated at 500ºC for 10 h in an evacuated silica tube. Because the Nd powder is reactive in air and a moist atmosphere, this process was carried out in an Ar-filled glovebox with a gas-purifier system. Then, a stoichiometric mixture of these starting materials was pressed into a pellet and heated for 15 h at 700ºC for $x \leq 0.4$ and at 650ºC for $x \geq 0.5$ in an evacuated silica tube. Notably, amounts of impurity phases, Bi_2Se_3 and Nd_2O_2Se, was significant when the samples with $x \geq 0.5$ were synthesized at 700 ºC.

2.2 Characterization

The chemical compositions of the obtained samples were examined using an energy dispersive X-ray spectrometer (EDX; Oxford, SwiftED3000). The phase purity and crystal structure of the samples were examined by synchrotron powder X-ray diffraction (SPXRD) performed at the BL02B2 beamline of SPring-8 (proposal numbers 2018A0074 and 2018B1246). The measurements were performed at 297 K. The diffraction data were collected using a high-resolution

one-dimensional semiconductor detector (multiple MYTHEN system) [28]. The wavelength of the radiation beam was determined to be 0.495274(1) Å (proposal number 2018A0074) and 0.496345(1) Å (No. 2018B1246) using a CeO_2 standard. The crystal structure parameters were refined by the Rietveld method using RIETAN-FP software [29]. The crystal structure was visualized using VESTA software [30].

2.3 Transport measurement

Electrical resistivity at ambient pressure was measured using the four-probe method on a GM refrigerator system. Measurements of electrical resistance under high pressure were performed using an originally designed DAC with boron-doped diamond electrodes [25,31,32] on the bottom anvil of nanopolycrystalline diamond [33], as shown in Fig. 2. The sample was placed on the boron-doped diamond electrodes in the center of the bottom anvil. The surface of the bottom anvil except for the sample space and electrical terminal were covered by the undoped diamond insulating layer. The cubic boron nitride powders with ruby manometer were used as a pressure-transmitting medium. The applied pressure was estimated by the fluorescence from ruby powders [34] and the Raman spectrum from the culet of top diamond anvil [35] by an inVia Raman Microscope (RENISHAW). The resistance was measured by a standard four-probe method on a Physical Property Measurement System (Quantum Design: PPMS).

3. Results and discussion

3.1 Crystal structure and chemical composition

Figure 3(a) shows the SPXRD pattern and Rietveld fitting results for x = 0.7 as a representative data. Almost all the diffraction peaks can be assigned to those of the tetragonal *P4/nmm* space group, indicating that the obtained sample is mainly composed of $NdO_{0.8}F_{0.2}Sb_{1-x}Bi_xSe_2$-type phase. However, several peaks, attributable to impurity phases, Nd_2O_2Se (4.1 wt%), NdOF (1.9 wt%), and Bi_2Se_3 (0.8 wt%), were also observed. At the same time, the diffraction peaks for other samples can also be assigned to those of the tetragonal *P4/nmm* space group, as shown in Fig. S1 [36]. Amounts of secondary phases are significant for x = 0.8, Nd_2O_2Se (13.2 wt%) and Bi_2Se_3 (12.9 wt%), suggesting solubility limit of Bi for Sb in $NdO_{0.8}F_{0.2}Sb_{1-x}Bi_xSe_2$ is at around this composition. Figure 3(b) shows the chemical composition ratios of Nd, Sb, Bi, and Se determined using EDX. The results indicate that the chemical compositions of the obtained samples are in reasonable agreement with the nominal compositions of the starting materials.

Figure 3(c) depicts the calculated lattice parameters. The lattice parameter a increased almost linearly with increasing x owing to the larger ionic radius of Bi ions than that of Sb ions (Channon's five-coordinate ionic radius, r_{Bi}^{3+} = 96 pm and r_{Sb}^{3+} = 80 pm) [37]. On the other hand, the c exhibits anomalous change at around x = 0.5–0.6. Although the origin of this deviation from linear relationship between c and x is not clear yet, it seems to be correlated to electrical carrier transport of the present samples, as described below. Note that c-axis length tends to correlate with amount of electron doping in the $BiCh_2$-based systems [2-8].

Figures 4(a)-(d) show selected bond distances and angle. Bond distances for in-plane Bi/Sb

(Pn)-Se1 and Pn-Se2 increased almost linearly with increasing *x*, consistent with an increase in lattice parameters. On the other hand, interplane Pn-Se1 distance is in 3.43 ± 0.03 Å for all of examined samples. As a result, Se1-Pn-Se1 bond angle tends to decrease with increasing *x*. This indicates that $PnSe_2$ conducting layer is corrugated by Bi doping. The Se1-Pn-Se1 bond angle can be classified into two groups, namely, Se1-Pn-Se1 bond angle of ca. 171° for Sb-rich composition ($x \leq 0.3$), and of ca. 169° for Bi-rich composition ($x \geq 0.6$). The temperature dependence of electrical resistivity near room temperature turns from insulating to metallic behavior at the intermediate region, $x = 0.4–0.5$.

3.2 Transport property under ambient pressure

Figure 5(a) shows the temperature dependences of electrical resistivity measured under ambient pressure. For $x = 0$, electrical resistivity increased with decreasing temperature, leading to ~10^5 Ωcm at 2 K. This insulating behavior is suppressed by Bi doping. Temperature dependence of electrical resistivity near room temperature turns from insulating to metallic behavior at $x = 0.5–0.6$, in which anomalous change of *c*-axis length and Se1-Pn-Se1 bond angle is observed. Notably, weakly localized behavior is still observed at low temperature for all samples. For example, electrical resistivity increases with decreasing temperature below 20 K for $x = 0.8$, as shown in Fig. 5(b).

3.3 Transport property under high pressure

To investigate the electrical transport under high pressure, we employed x = 0.3 and 0.7 as the representatives of Sb-rich and Bi-rich composition, respectively. It should be noted that x = 0.8 is ruled out for high pressure measurements because of the existence of nonnegligible amount of Bi_2Se_3 secondary phase (12.9 wt%), which shows superconductivity under high pressure [38,39].

Figure 6 shows the temperature dependences of electrical resistance for x = 0.3 under various pressures (a) from 12.2 GPa to 50 GPa, and (b) from 50 GPa to 90 GPa. The resistance exhibits an insulating behavior with a negative slope of dR/dT up to 42.5 GPa, although it decreases with increasing pressure. A sudden drop of resistance was observed at 5.1 K at 50 GPa, corresponding to a superconducting transition. At 57.2 GPa, the resistance at 10 K decreases about four orders in magnitude as compared to that at 12.2 GPa, indicating the insulator to metal transition at this pressure. The resistance continued to decrease up to 90 GPa, and then, the diamond anvil was broken. It should be noted that zero resistivity was not observed at low temperature, most likely due to inhomogeneity of applied pressure for polycrystalline sample, which is generally occurred with DAC systems [40].

Figure 6(c) shows resistance below 10 K for x = 0.3 under various pressures from 50 GPa to 90 GPa. We first observed the superconducting transition with T_c^{onset} = 5.1 K under 50 GPa. The T_c^{onset} was enhanced with an increase of applied pressure up to 70.8 GPa, reaching the maximum T_c^{onset} of 7.8 K. Under further compression, the T_c^{onset} was gradually decreased.

To confirm that the observed drop of resistance was originated from the superconductivity, we measured the resistance under magnetic fields. Figure 7 shows temperature dependences of

resistance for x = 0.3 in magnetic fields under representative pressures of (a) 50 GPa, (b) 70.8 GPa, and (c) 90 GPa. The drops of resistance is gradually suppressed by an increase of applied magnetic field, indicating the drops of resistance come from the superconductivity. The insets show the temperature dependences of upper critical field H_{c2} estimated from the Werthamer-Helfand-Hohenberg (WHH) approximation for type II superconductors in a dirty limit [41]. The $H_{c2}(0)$ at 70.8 GPa was estimated to be 6.6 T, which is comparable to that of $BiCh_2$-based superconductors. Notably, the lower $H_{c2}(0)$ at 90 GPa, 4.0 T, than that at 70.8 GPa is consistent with lower T_c at this pressure.

Figure 8(a) shows temperature dependences of resistance in Bi-rich sample, x = 0.7, under pressures from 0.6 GPa to 52 GPa. An insulating behavior was observed as same as x = 0.3 up to 36.5 GPa, while resistivity of x = 0.7 measured at ambient pressure shows metallic behavior at temperatures between 100 and 300 K (see Fig. 5(b)). This is probably due to weak coupling between grain boundary, because the measurements under high pressure are performed on polycrystalline powder samples. The drop of resistance corresponding to the superconducting transition was observed at 5.9 K at 43.5 GPa. These critical parameters to induce superconductivity, temperature and pressure, are almost comparable to those of x = 0.3. Figures 8(b) and 8(c) show the temperature dependences of resistance in x = 0.7 under magnetic fields at (b) 43.5 GPa and (c) 52.0 GPa. Again, suppression of drops in resistance by applying magnetic field indicate that this corresponds to a superconducting transition. The $H_{c2}(0)$ of x = 0.7 was evaluated to be 9.6 T and 10.8 T at 43.5 GPa and 52.0 GPa, respectively. These are distinctly higher than that of x = 0.3.

Figures 9(a) and 9(b) show pressure-phase diagrams for T_c^{onset} and resistances at 200 K and 10 K for x = 0.3 and 0.7. In spite of different Sb/Bi substitutional ratio, both compositions exhibited quite similar responses against the applied pressures. Namely, critical pressure to induce superconductivity is as high as ~45 GPa for both the Sb rich (x = 0.3) and Bi rich (x = 0.7) composition, which seems to contradict to our simple expectation that superconductivity is more easily induced under high pressure in Bi rich sample, because of its metallic-like nature at ambient pressure. We deduce this is due to lattice instability in the present compounds. All of the crystal structure of the samples presented in this study is assigned to tetragonal *P*4/*nmm* space group using SPXRD measured at room temperature. However, theoretical studies show that the existence of imaginary phonons in the related compounds [10,42-45]. These studies also reported that the total energy of the tetragonal *P*4/*nmm* is not the lowest [43,44]. Indeed, symmetry lowering to monoclinic $P2_1/m$ [46-48] and nanoscale atomic distortion [49-54] have been experimentally observed for $BiCh_2$-based compounds. For another layered compound, R_2O_2Pn with a Pn^{2-} net, insulating nature that originates from lattice distortion has recently been investigated [55-60]. Although both R_2O_2Bi and R_2O_2Sb are expected to be a metallic owing to −2 valence state of Pn, R_2O_2Sb is an insulator, most likely due to the gap arising from the lattice instability [58]. It may be possible that such gap also exists in the present $SbSe_2$-based compounds.

4. Conclusion

We synthesized Bi-substituted $SbCh_2$-based compounds $NdO_{0.8}F_{0.2}Sb_{1-x}Bi_xSe_2$ (x = 0–0.8)

and demonstrated in-situ transport measurements under high pressure condition to examine the pressure-induced superconductivity. In Sb-rich composition, x = 0.3, a superconducting transition with T_c^{onset} = 5.3 K was observed at 50 GPa, and reached 7.9 K at 70.8 GPa. The $H_{c2}(0)$ was estimated to be 6.6 T at 70.8 GPa using WHH model. For Bi-rich one (x = 0.7), a superconducting transition with T_c^{onset} = 5.9 K was observed at 43.5 GPa, which is the almost comparable to that of x = 0.3. The present work will be helpful to bridge the gap between insulating $SbCh_2$-based and metallic $BiCh_2$-based systems, which show superconductivity at ambient pressure.

Acknowledgment

We thank fruitful discussion with K. Kuroki, M. Ochi, H. Usui, and N. Hirayama (Osaka University). This work was partly supported by JST CREST Grant No. JPMJCR16Q6, JST-Mirai Program Grant Number JPMJMI17A2, JSPS KAKENHI Grant Number 17J05926, 17H05481, 15H05886, and 16H04493, and Iketani Science and Technology Foundation (No. 0301042-A), Japan. A part of the fabrication process of diamond electrodes was supported by NIMS Nanofabrication Platform in Nanotechnology Platform Project sponsored by the Ministry of Education, Culture, Sports, Science and Technology (MEXT), Japan. The part of the high pressure experiments was supported by the Visiting Researcher's Program of Geodynamics Research Center, Ehime University.

References

[1] Y. Mizuguchi, H. Fujihisa, Y. Gotoh, K. Suzuki, H. Usui, K. Kuroki, S. Demura, Y. Takano, H. Izawa, O. Miura, Phys. Rev. B **86**, 220510(R) (2012).

[2] Y. Mizuguchi, S. Demura, K. Deguchi, Y. Takano, H. Fujihisa, Y. Gotoh, H. Izawa, and O. Miura, J. Phys. Soc. Jpn. **81**, 114725 (2012).

[3] Y. Mizuguchi, J. Phys. Soc. Jpn. **88**, 041001 (2019).

[4] J. Xing, S. Li, X. Ding, H. Yang, and H. H. Wen, Phys. Rev. B **86**, 214518 (2012).

[5] S. Demura, K. Deguchi, Y. Mizuguchi, K. Sato, R. Honjyo, A. Yamashita, T. Yamaki, H. Hara, T. Watanabe, S. J. Denholme, M. Fujioka, H. Okazaki, T. Ozaki, O. Miura, T. Yamaguchi, H. Takeya, and Y. Takano, J. Phys. Soc. Jpn. **84**, 024709 (2015).

[6] R. Jha, A. Kumar, S. K. Singh, and V. P. S. Awana, J. Supercond. Novel Magn. **26**, 499 (2013).

[7] S. Demura, Y. Mizuguchi, K. Deguchi, H. Okazaki, H. Hara, T. Watanabe, S. J. Denholme, M. Fujioka, T. Ozaki, H. Fujihisa, Y. Gotoh, O. Miura, T. Yamaguchi, H. Takeya, and Y. Takano, J. Phys. Soc. Jpn. **82**, 033708 (2013).

[8] D. Yazici, K. Huang, B. D. White, A. H. Chang, A. J. Friedman, and M. B. Maple, Philos. Mag. **93**, 673 (2013).

[9] Y. Mizuguchi, T. Hiroi, J. Kajitani, H. Takatsu, H. Kadowaki, and O. Miura, J. Phys. Soc. Jpn. **83**, 53704 (2014).

[10] X. Wan, H. C. Ding, S. Savrasov, and C. G. Duan, Phys. Rev. B **87**, 115124 (2013).

[11] S. F. Wu, P. Richard, X. B. Wang, C. S. Lian, S. M. Nie, J. T. Wang, N. L. Wang, and H.

Ding, Phys. Rev. B **90**, 54519 (2014).

[12] G. Lamura, T. Shiroka, P. Bonf, S. Sanna, R. De Renzi, C. Baines, H. Luetkens, J. Kajitani, Y. Mizuguchi, O. Miura, K. Deguchi, S. Demura, Y. Takano, and M. Putti, Phys. Rev. B **88**, 180509 (2013).

[13] T. Yamashita, Y. Tokiwa, D. Terazawa, M. Nagao, S. Watauchi, I. Tanaka, T. Terashima, and Y. Matsuda, J. Phys. Soc. Japan **85**, 73707 (2016).

[14] C. Morice, R. Akashi, T. Koretsune, S. S. Saxena, and R. Arita, Phys. Rev. B **95**, 180505 (2017).

[15] Y. Ota, K. Okazaki, H. Q. Yamamoto, T. Yamamoto, S. Watanabe, C. Chen, M. Nagao, S. Watauchi, I. Tanaka, Y. Takano, and S. Shin, Phys. Rev. Lett. **118**, 167002 (2017).

[16] K. Hoshi, Y. Goto, and Y. Mizuguchi, Phys. Rev. B **97**, 094509 (2018).

[17] H. Usui, K. Suzuki, and K. Kuroki, Phys. Rev. B **86**, 220501 (2012).

[18] K. Suzuki, H. Usui, K. Kuroki, T. Nomoto, K. Hattori, and H. Ikeda, J. Phys. Soc. Jpn. **88**, 041008 (2019).

[19] M. Ochi, H. Usui, and K. Kuroki, Phys. Rev. Appl. **8**, 064020 (2017).

[20] X.-Y. Dong, J.-F. Wang, R.-X. Zhang, W.-H. Duan, B.-F. Zhu, J. O. Sofo, and C.-X. Liu, Nat. Commun. **6**, 8517 (2015).

[21] M. Ochi, H. Usui, and K. Kuroki, J. Phys. Soc. Jpn. **88**, 041010 (2019).

[22] Y. Goto, A. Miura, R. Sakagami, Y. Kamihara, C. Moriyoshi, Y. Kuroiwa, and Y. Mizuguchi, J. Phys. Soc. Jpn. **87**, 074703 (2018).

[23] M. Nagao, M. Tanaka, R. Matsumoto, H. Tanaka, S. Watauchi, Y. Takano, and I. Tanaka, Cryst. Growth Des. **16**, 3037 (2016).

[24] M. Nagao, M. Tanaka, A. Miura, M. Kitamura, K. Horiba, S. Watauchi, Y. Takano, H. Kumigashira, and I. Tanaka, Solid State Commun. **289**, 38 (2019).

[25] R. Matsumoto, M. Nagao, M. Ochi, H. Tanaka, H. Hara, S. Adachi, K. Nakamura, R. Murakami, S. Yamamoto, T. Irifune, H. Takeya, I. Tanaka, K. Kuroki, and Y. Takano, J. Appl. Phys. **125**, 075102, (2019).

[26] Y. Goto, A. Miura, C. Moriyoshi, Y. Kuroiwa, and Y. Mizuguchi, J. Phys. Soc. Jpn. **88**, 024705 (2019).

[27] Y. Mizuguchi, A. Miura, J. Kajitani, T. Hiroi, and O. Miura, Sci. Rep. **5**, 14968 (2015).

[28] S. Kawaguchi, M. Takemoto, K. Osaka, E. Nishibori, C. Moriyoshi, Y. Kubota, Y. Kuroiwa, K. Sugimoto, S. Kawaguchi, M. Takemoto, K. Osaka, E. Nishibori, C. Moriyoshi, and Y. Kubota, Rev. Sci. Instrum. **88**, 85111085119 (2017).

[29] F. Izumi and K. Momma, Solid State Phenom. **130**, 15 (2007).

[30] K. Momma and F. Izumi, J. Appl. Crystallogr. **41**, 653 (2008).

[31] R. Matsumoto, A. Yamashita, H. Hara, T. Irifune, S. Adachi, H. Takeya, and Y. Takano, Appl. Phys. Express **11**, 053101 (2018).

[32] R. Matsumoto, H. Hara, H. Tanaka, K. Nakamura, N. Kataoka, S. Yamamoto, T. Irifune, A. Yamashita, S. Adachi, H. Takeya, and Y. Takano, J. Phys. Soc. Jpn. **87**, 124706 (2018).

[33] T. Irifune, A. Kurio, S. Sakamoto, T. Inoue, and H. Sumiya, Nature **421**, 599 (2003).

[34] G. J. Piermarini, S. Block, J. D. Barnett, and R. A. Forman, J. Appl. Phys. **46**, 2774 (1975)

[35] Y. Akahama and H. Kawamura, J. Appl. Phys. **96**, 3748 (2004).

[36] See Supplemental Material at [*URL will be inserted by publisher*] for SPXRD patterns of $NdO_{0.8}F_{0.2}Sb_{1-x}Bi_xSe_2$.

[37] R. D. Shannon, Acta Crystallogr. **A32**, 751 (1976).

[38] K. Kirshenbaum, P. S. Syers, A. P. Hope, N. P. Butch, J. R. Jeffries, S. T. Weir, J. J. Hamlin, M. B. Maple, Y. K. Vohra, and J. Paglione, Phys. Rev. Lett. **111**, 087001 (2013).

[39] P. P. Kong, J. L. Zhang, S. J. Zhang, J. Zhu, Q. Q. Liu, R. C. Yu, Z. Fang, C. Q. Jin, W. G. Yang, X. H. Yu, J. L. Zhu, and Y. S. Zhao, J. Phys.: Condens. Matter. **25**, 362204 (2013).

[40] T. Tomita, M. Ebata, H. Soeda, H. Takahashi, H. Fujihisa, Y. Gotoh, Y. Mizuguchi, H. Izawa, O. Miura, S. Demura, K. Deguchi, and Y. Takano, J. Phys. Soc. Japan **83**, 063704 (2014).

[41] N. R. Werthamer, E. Helfand, and P. C. Hohemberg, Phys. Rev. **147**, 295 (1966).

[42] B. Li, Z. W. Xing, and G. Q. Huang, Europhys. Lett. **101**, 47002 (2013).

[43] Q. Liu, X. Zhang, and A. Zunger, Phys. Rev. B **93**, 174119 (2016).

[44] T. Yildirim, Phys. Rev. B **87**, 020506 (2013).

[45] X. Wan, H.-C. Ding, S. Y. Savrasov, and C.-G. Duan, Phys. Rev. B **87**, 115124 (2013).

[46] R. Sagayama, H. Sagayama, R. Kumai, Y. Murakami, T. Asano, J. Kajitani, R. Higashinaka, T. D. Matsuda, and Y. Aoki, J. Phys. Soc. Jpn. **84**, 123703 (2015).

[47] T. Tomita, M. Ebata, H. Soeda, H. Takahashi, H. Fujihisa, Y. Gotoh, Y. Mizuguchi, H. Izawa, O. Miura, S. Demura, K. Deguchi, and Y. Takano, J. Phys. Soc. Jpn. **83**, 063704 (2014).

[48] K. Nagasaka, A. Nishida, R. Jha, J. Kajitani, O. Miura, R. Higashinaka, T. D. Matsuda, Y. Aoki, A. Miura, C. Moriyoshi, Y. Kuroiwa, H. Usui, K. Kuroki, and Y. Mizuguchi, J. Phys. Soc. Jpn. **86**, 074701 (2017).

[49] A. Athauda, J. Yang, S.-H. Lee, Y. Mizuguchi, K. Deguchi, Y. Takano, O. Miura, and D. Louca, Phys. Rev. B 91, 144112 (2015).

[50] A. Athauda, J. Yang, B. Li, Y. Mizuguchi, S.-H. Lee, and D. Louca, J. Supercond. Novel Magn. 28, 1255 (2015).

[51] A. Athauda, Y. Mizuguchi, M. Nagao, J. Neuefeind, and D. Louca, J. Phys. Soc. Jpn. 86, 124718 (2017).

[52] A. Athauda, C. Hoffmann, S. Aswartham, J. Terzic, G. Cao, X. Zhu, Y. Ren, and D. Louca, J. Phys. Soc. Jpn. 86, 054701 (2017).

[53] A. Athauda and D. Louca, J. Phys. Soc. Jpn. **88**, 041004 (2019).

[54] Y. Mizuguchi, E. Paris, T. Sugimoto, A. Iadecola, J. Kajitani, O. Miura, T. Mizokawa, and N. L. Saini, Phys. Chem. Chem. Phys. **17**, 22090 (2015).

[55] J. Nuss and M. Jansen, J. Alloys Compd. **480**, 57 (2009).

[56] H. Mizoguchi and H. Hosono, J. Am. Chem. Soc. **133**, 2394 (2011).

[57] P. L. Wang, T. Kolodiazhnyi, J. Yao, and Y. Mozharivskyj, J. Am. Chem. Soc. **134**, 1426 (2012).

[58] H. Kim, C. Kang, K. Kim, J. H. Shim, and B. I. Min, Phys. Rev. B **91**, 165130 (2015).

[59] H. Kim, C. Kang, K. Kim, J. H. Shim, and B. I. Min, Phys. Rev. B **93**, 125116 (2016).

[60] R. Sei, S. Kitani, T. Fukumura, H. Kawaji, and T. Hasegawa, J. Am. Chem. Soc. **138**, 11085 (2016).

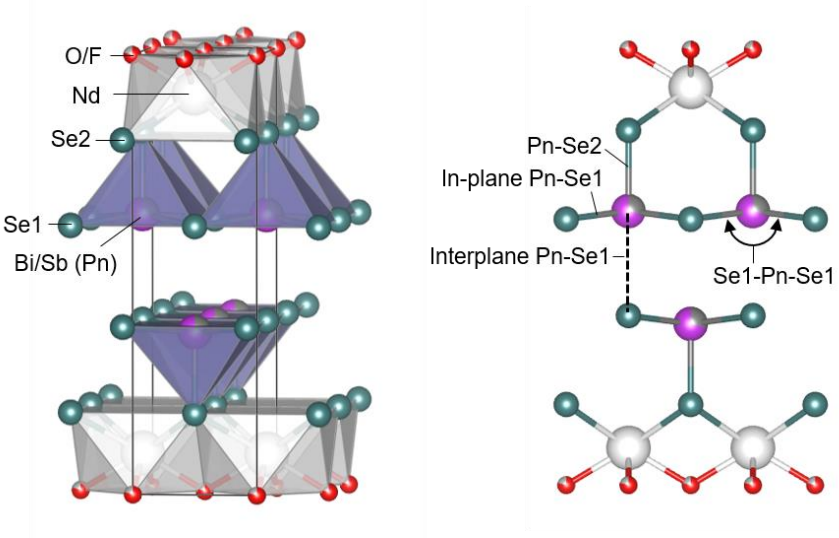

FIG. 1. Crystal structure of $NdO_{0.8}F_{0.2}Sb_{1-x}Bi_xSe_2$ (x = 0.3) which belongs to tetragonal *P*4/*nmm* space group. The black line denotes the unit cell. Se ions have two crystallographic sites: in-plane (Se1) and out-of-plane (Se2). Pnictogen (Sb and Bi) is denoted as Pn.

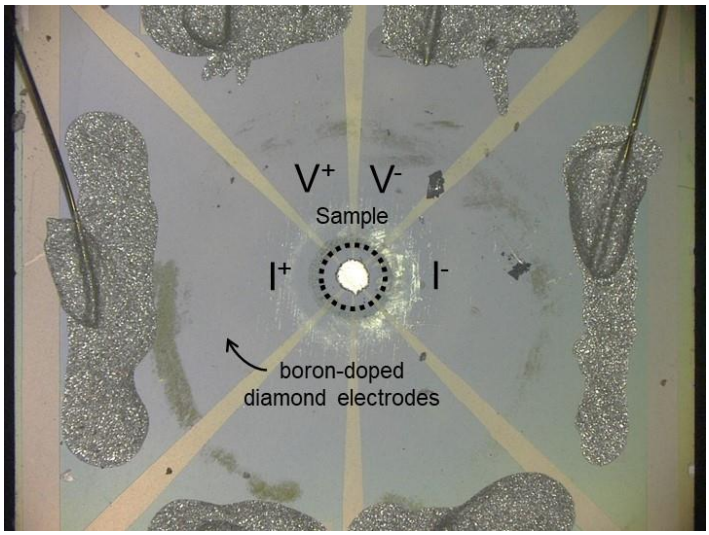

FIG. 2. Optical image of the sample space of DAC with boron-doped diamond electrodes.

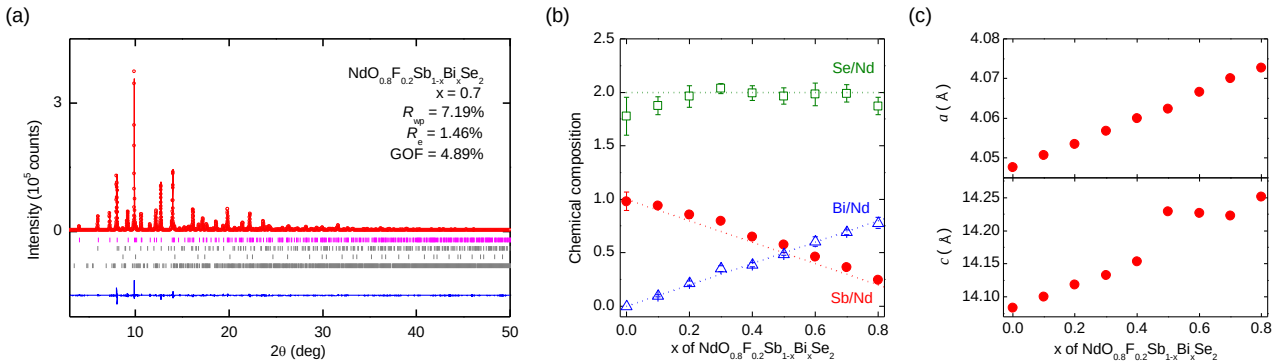

FIG. 3. (a) SPXRD pattern and Rietveld fitting results for x = 0.7 as a representative data of $NdO_{0.8}F_{0.2}Sb_{1-x}Bi_xSe_2$. The measurement was performed at 297 K. The wavelength of the radiation beam was determined to be 0.496345(1) Å. The circles and solid curve represent the observed and calculated patterns, respectively, and the difference between the two is shown at the bottom. The vertical marks indicate the Bragg diffraction positions for $NdO_{0.8}F_{0.2}Sb_{0.3}Bi_{0.7}Se_2$, Nd_2O_2Se, NdOF, and Sb_2Se_3, from top to bottom, respectively. SPXRD patterns of other samples are shown in Supplemental Material [36]. (b) Calculated lattice parameters from Rietveld refinement. (c) Chemical composition ratios of Nd, Sb, Bi, and Se determined using EDX.

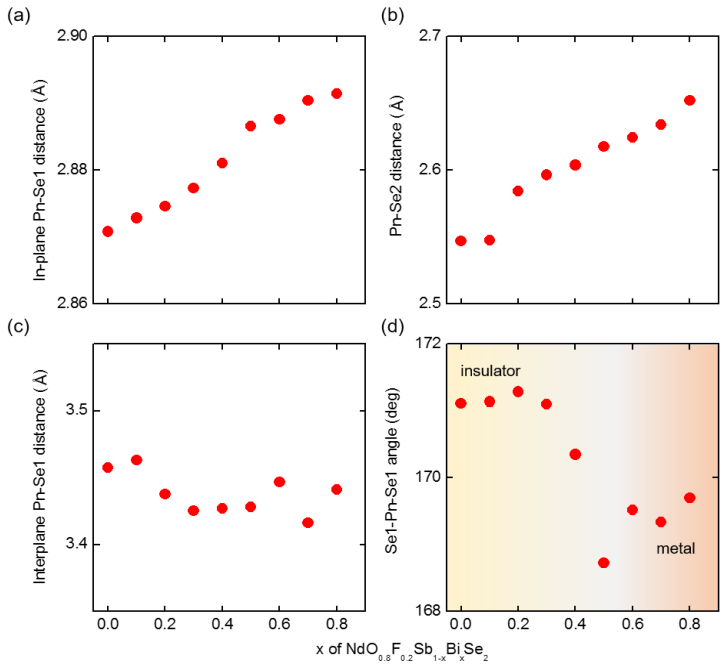

FIG. 4. Selected bond distances and angle for $NdO_{0.8}F_{0.2}Sb_{1-x}Bi_xSe_2$: (a) in-plane Pn-Se1 distance, (b) Pn-Se2 distance, (c) interplane Pn-Se1 distance, and (d) Se1-Pn-Se1 angle. The error bars are less than the size of the symbols.

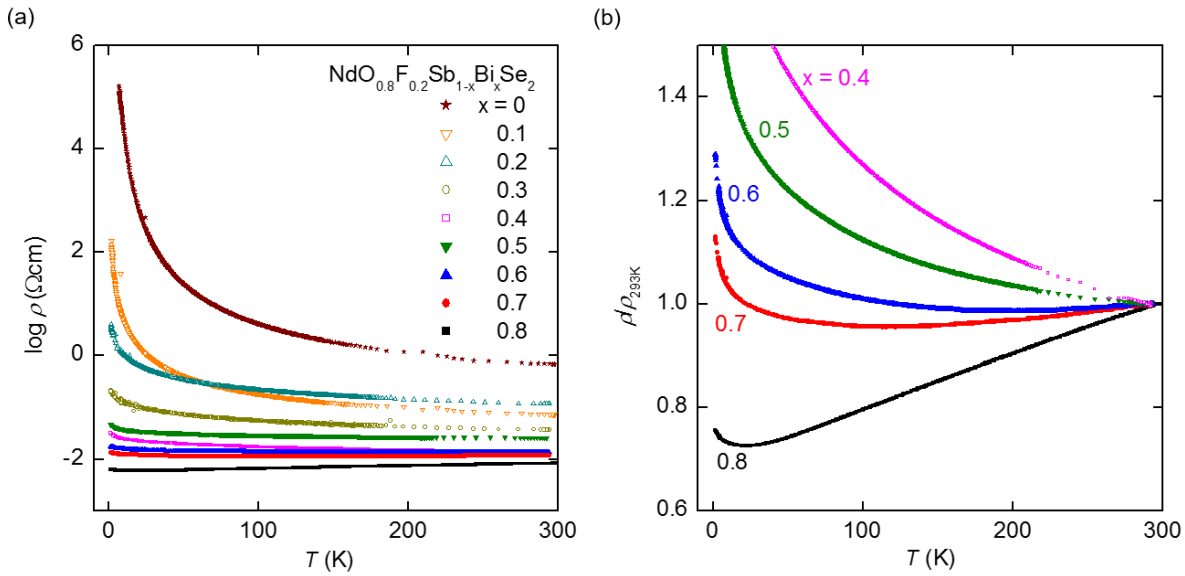

FIG. 5. (a) Temperature (T) dependence of logarithmic resistivity (ρ) in $NdO_{0.8}F_{0.2}Sb_{1-x}Bi_xSe_2$ (x = 0, 0.1, 0.2, 0.3, 0.4, 0.5, 0.6, 0.7, 0.8) measured at ambient pressure. (b) Normalized ρ vs. T for x = 0.4–0.8.

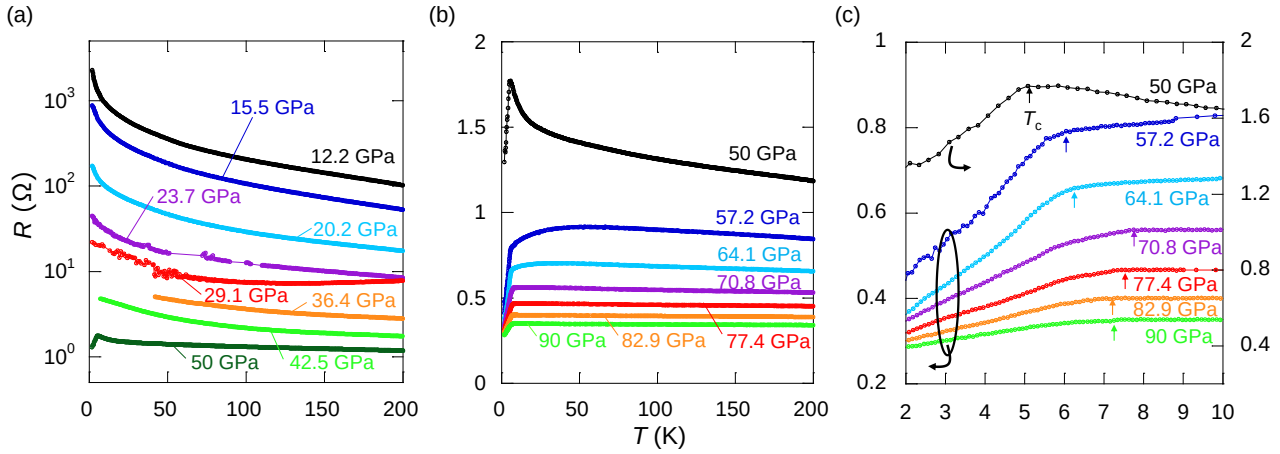

FIG. 6. Temperature dependence of resistance in x = 0.3 under various pressures (a) from 12.2 GPa to 50 GPa, and (b) from 50 GPa to 90 GPa. (c) Enlarged plots around superconducting transitions for temperature dependence of resistance under various pressure from 50 GPa to 90 GPa.

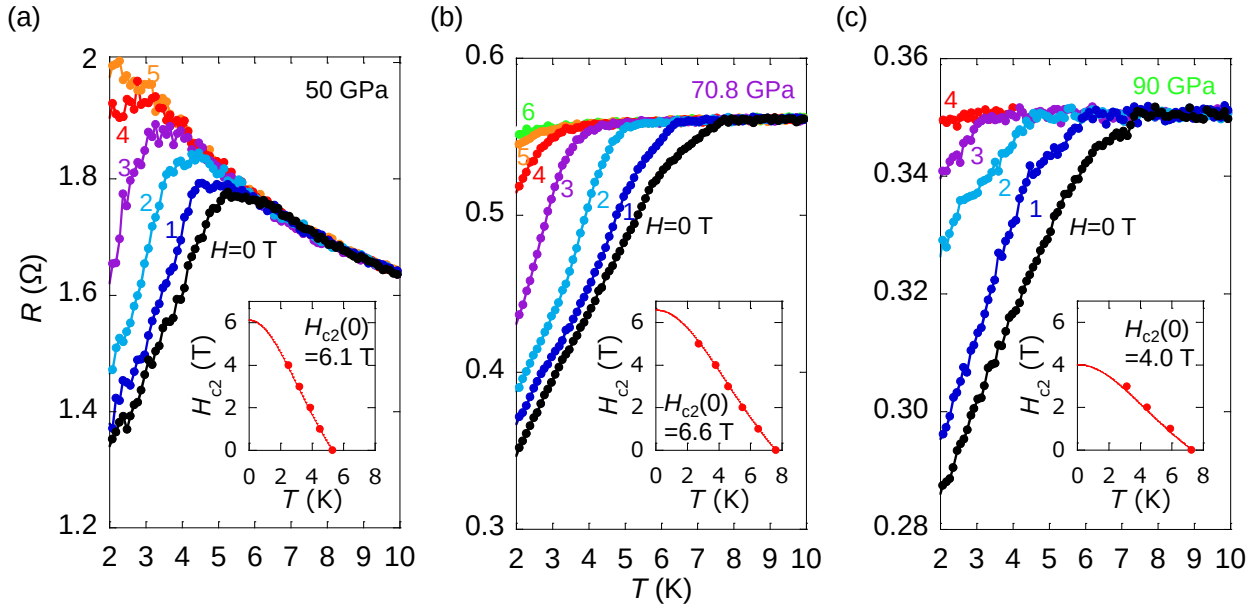

FIG. 7. Temperature dependence of resistance in x = 0.3 in magnetic fields under (a) 50 GPa, (b) 70.8 GPa, and (c) 90 GPa. The insets show magnetic field–temperature phase diagram. Solid line was calculated using WHH model.

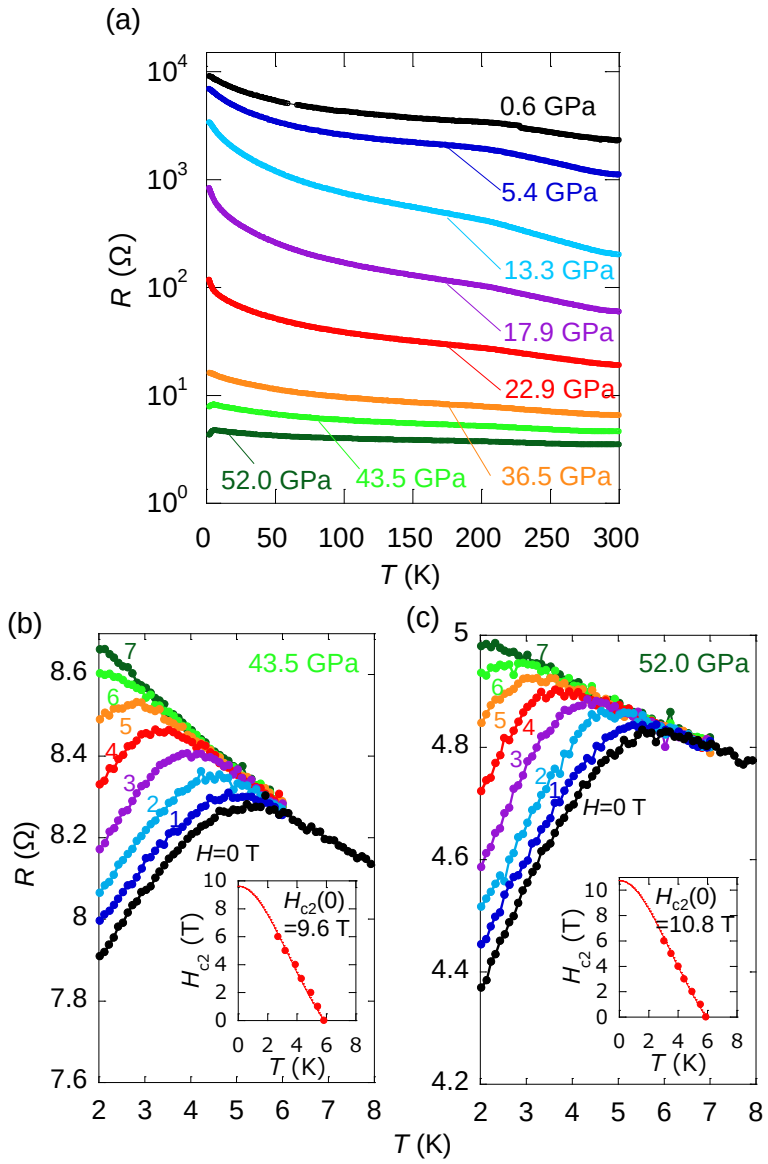

FIG. 8. (a) Temperature dependence of resistance in x = 0.7 under various pressure from 0.6 GPa to 52 GPa. (b,c) Temperature dependence of resistance in magnetic fields under (b) 43.5 GPa, and (c) 52 GPa.

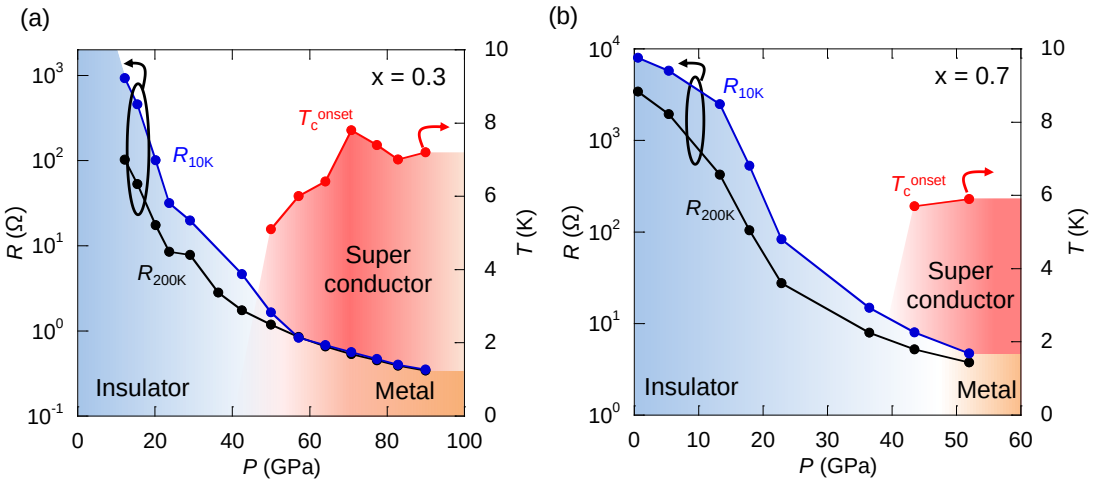

Figure 9. (a) Pressure-phase diagrams for T_c^{onset}, resistance at 200 K and 10 K for (a) x = 0.3 and (b) x = 0.7.

Supplemental Materials for

"Pressure-induced superconductivity in layered pnictogen diselenide $NdO_{0.8}F_{0.2}Sb_{1-x}Bi_xSe_2$ (x = 0.3 and 0.7)"

Ryo Matsumoto,[1,2] Yosuke Goto,[3] Sayaka Yamamoto,[1,2,4] Kenta Sudo,[3] Akira Miura,[5] Chikako Moriyoshi,[6] Yoshihiro Kuroiwa,[6] Shintaro Adachi,[1] Tetsuo Irifune,[7] Hiroyuki Takeya,[1] Hiromi Tanaka,[4] Yoshikazu Mizuguchi,[3] and Yoshihiko Takano[1,2]

[1]*National Institute for Materials Science, 1-2-1 Sengen, Tsukuba, Ibaraki 305-0047, Japan*

[2]*University of Tsukuba, 1-1-1 Tennodai, Tsukuba, Ibaraki 305-8577, Japan*

[3]*Department of Physics, Tokyo Metropolitan University, 1-1 Minami-osawa, Hachioji, Tokyo 192-0397, Japan*

[4]*National Institute of Technology, Yonago College, 4448 Hikona, Yonago, Tottori 683-8502, Japan*

[5] *Faculty of Engineering, Hokkaido University, Kita 13, Nishi 8 Sapporo 060-8628, Japan*

[6] *Department of Physical Science, Hiroshima University, 1-3-1 Kagamiyama, Higashihiroshima, Hiroshima 739-8526, Japan*

[7]*Geodynamics Research Center, Ehime University, Matsuyama, Ehime 790-8577, Japan*

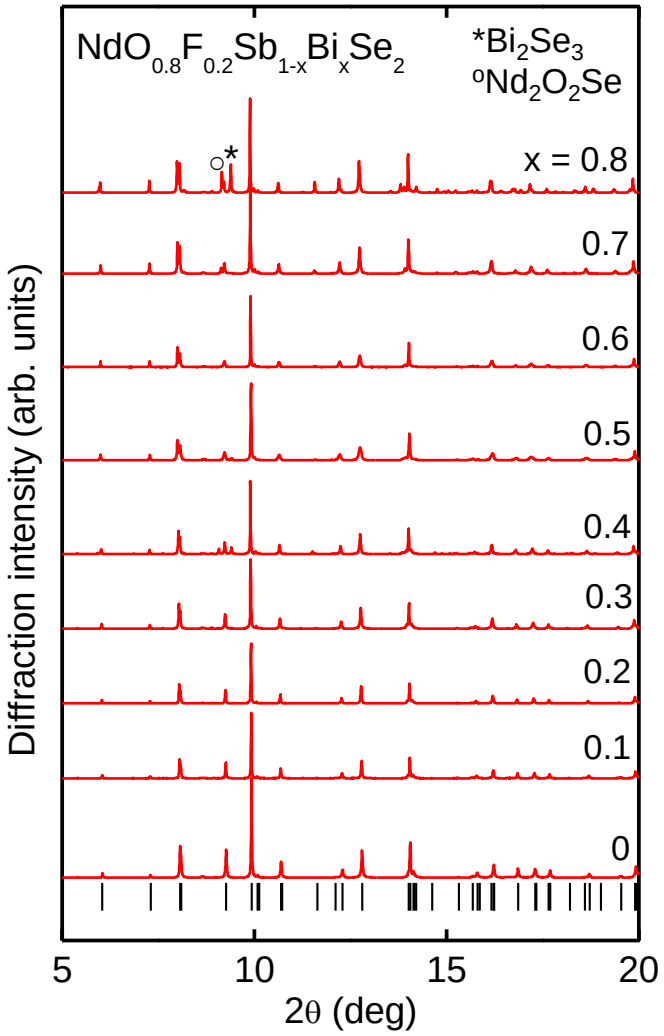

FIG. S1. SPXRD patterns of $NdO_{0.8}F_{0.2}Sb_{1-x}Bi_xSe_2$. The vertical marks at the bottom show the Bragg diffraction angles of $NdO_{0.8}F_{0.2}SbSe_2$. The asterisk and open circle represent the diffraction peaks due to Bi_2Se_3 and Nd_2O_2Se, respectively.